Author/s:
Piacentino, EL;Parker, K;Gilbert, TM;O'Hair, RAJ;Ryzhov, V

Title:
Role of Ligand in the Selective Production of Hydrogen from Formic Acid Catalysed by the Mononuclear Cationic Zinc Complexes [(L)Zn(H)]+ (L=tpy, phen, and bpy)

Date:
2019-07-25

Citation:
Piacentino, E. L., Parker, K., Gilbert, T. M., O'Hair, R. A. J. & Ryzhov, V. (2019). Role of Ligand in the Selective Production of Hydrogen from Formic Acid Catalysed by the Mononuclear Cationic Zinc Complexes [(L)Zn(H)]+ (L=tpy, phen, and bpy). Chemistry A European Journal, 25 (42), pp.9959-9966. https://doi.org/10.1002/chem.201901360.

Persistent Link:
https://hdl.handle.net/11343/286089

Title: Role of ligand in the selective production of hydrogen from formic acid catalysed by the mononuclear cationic zinc complexes [(L)Zn(H)]+ (L = tpy, phen, and bpy).

Authors: Elettra L Piacentino; Kevin Parker; Thomas M. Gilbert; Richard A. J. O'Hair; Victor Ryzhov, Ph.D.

To be cited as: 10.1002/chem.201901360

Link to VoR: https://doi.org/10.1002/chem.201901360

Role of ligand–in the selective production of hydrogen from formic acid catalysed by the mononuclear cationic zinc complexes $[(L)Zn(H)]^+$ (L = tpy, phen, and bpy).

Elettra L. Piacentino,[1] Kevin Parker,[1] Thomas M. Gilbert,[1] Richard A. J. O'Hair,[2*] and Victor Ryzhov.[1*]

[1] Department of Chemistry and Biochemistry, Northern Illinois University, DeKalb, IL, 60115, USA

[2] School of Chemistry and Bio21 Molecular Science and Biotechnology Institute, The University of Melbourne, Parkville, Victoria 3010, Australia

Abstract:

A series of zinc-based catalysts was evaluated for their efficiency in decomposing formic acid into molecular hydrogen and carbon dioxide in the gas phase using quadrupole ion trap mass spectrometry experiments. The effectiveness of the catalysts in the series $[(L)Zn(H)]^+$, where L = 2,2′:6′,2″-terpyridine (tpy), 1,10-phenanthroline (phen) or 2,2'-bipyrydine (bpy) was found to depend on the ligand used, which turned out to be fundamental in tuning the catalytic properties of the zinc complex. Specifically, $[(tpy)Zn(H)]^+$ displayed the fastest reaction with formic acid proceeding via dehydrogenation to produce the zinc formate complex $[(tpy)Zn(O_2CH)]^+$ and H_2. The catalysts $[(L)Zn(H)]^+$ are reformed by decarboxylating the zinc formate complexes $[(L)Zn(O_2CH)]^+$ via collision-induced dissociation, which is the only reaction channel for each of the ligands used. The decarboxylation reaction was found to be reversible, since the zinc hydride complexes $[(L)Zn(H)]^+$ react with carbon dioxide yielding the zinc formate complex. This reaction was again substantially faster for L= tpy than L = phen or bpy. The energetics and mechanisms of these processes were modelled using several levels of density functional theory (DFT) calculations. Experimental results are fully supported by the computational predictions.

Keywords: Zinc catalysts • Formic Acid • Hydrogen storage • Mass Spectrometry • DFT calculations

Introduction

The decomposition of formic acid has been widely studied over the past century.[1] In the absence of a catalyst, pyrolysis of formic acid proceeds via two primary pathways: decarboxylation (Eq. 1) and dehydration (Eq. 2). These reactions are coupled by the water-gas shift reaction (Eq. 3),[2] and have been widely studied experimentally [3] and theoretically.[4] In the gas phase, the dehydration channel (Eq. 2) is the dominant reaction,[3] consistent with a lower activation energy, as predicted from DFT calculations. [4] Formic acid has been identified as a promising candidate for hydrogen storage applications,[5] requiring the development of catalysts that show selectivity for decarboxylation (Eq. 1).[6]

$$HCO_2H \rightarrow H_2 + CO_2 \quad \text{(Eq. 1)}$$

$$HCO_2H \rightarrow H_2O + CO \quad \text{(Eq. 2)}$$

$$H_2O + CO \rightarrow H_2 + CO_2 \quad \text{(Eq. 3)}$$

Over 100 years ago Sabatier pioneered the concept of using metal catalysts to selectively decompose formic acid. [1a,b] Early work was motivated in part by the advantage of the small size of formic acid, which allowed a detailed analysis of product pathways and yields and determination of activation energies with the available methods.[1] While these studies were largely of a fundamental nature, Sabatier's landmark opus on catalysis foreshadowed applications such as the use of formic acid as an in situ hydrogenation source for reduction of organic substrates.[1b] This concept has recently been adopted for the production of liquid hydrocarbon fuels by catalytic conversion of biomass-derived levulinic acid.[7]

The classes of metal catalysts that have been found to selectively decarboxylate formic acid (Eq. 1) include metal and metal oxide surfaces,[1c,d] mononuclear metal complexes,[6] metal clusters[8] and metal nanoparticles.[9] Since the precise molecular mechanisms that allow them to promote decarboxylation are often not well understood, other approaches are desirable. One such approach involves the use of gas-phase studies that employ multistage mass-spectrometry experiments in combination with DFT calculations[10] to probe the individual elementary steps of catalytic cycles.[11] Indeed, we have previously described two-step gas-phase catalytic cycles for the decarboxylation of formic acid involving metal hydride ion complex ions, $[(L)M_n(H)]^{+/-}$, which can be protonated by neutral formic acid in an ion-molecule reaction (IMR) to liberate H_2

and generate the metal formate complex ions, $[(L)M_n(O_2CH)]^{+/-}$ (Scheme 1A, Step **(I))**. The metal formate complexes can in turn be decarboxylated via collision-induced dissociation (CID) to reform the metal hydride catalyst (Scheme 1A, Step **(II)**). Examples of hydride catalysts that have been examined via this approach include magnesium hydride anions,[12] (Scheme 1B) and ligated binuclear coinage metal hydride cations, $[(L)M^1M^2(H)]^+$ (M = Cu, Ag, Au)[13] (Scheme 1C-E).

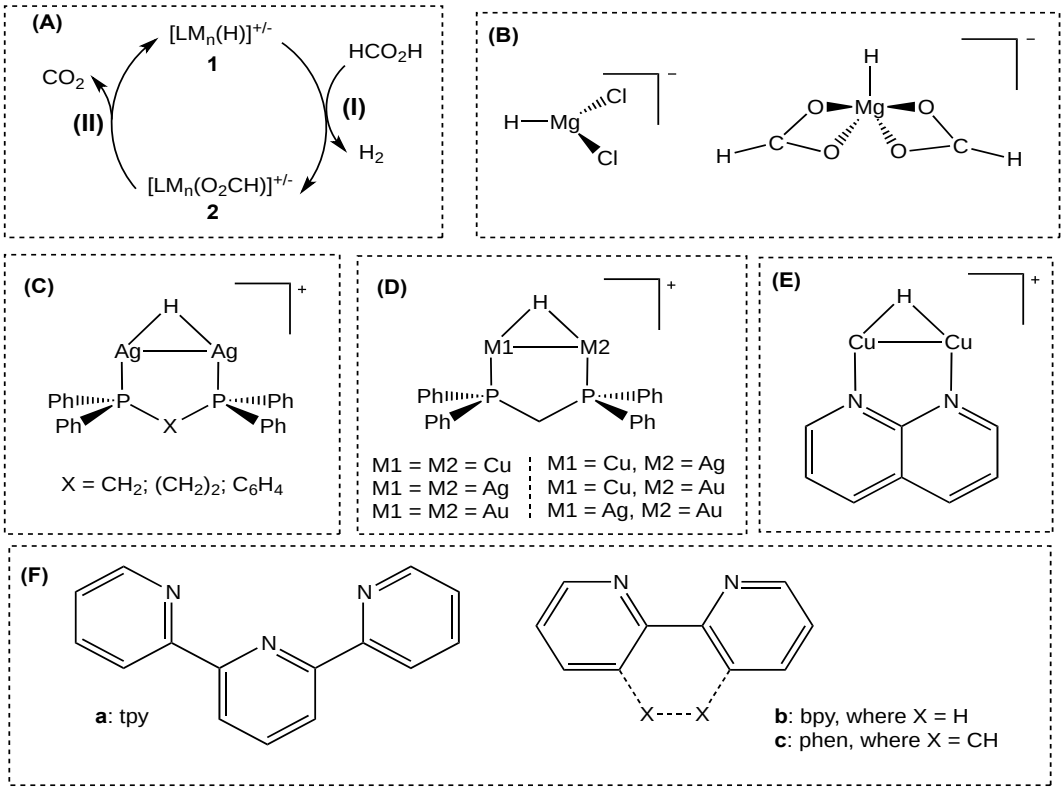

Scheme 1 (2 column) Selective decarboxylation of formic acid in the gas phase. **(a)** Two step catalytic cycle involving ligated metal hydride ions, $[(L)M_n(H)]^{+/-}$. Examples of $[(L)M_n(H)]^{+/-}$ studied: **(b)** magnesium hydride anion catalysts[12]; **(c)** binuclear silver catalysts[13a]; **(d)** binuclear coinage metal catalysts[13b]; **(e)** binuclear copper catalyst[13c] ; **(f)** $[(L)Zn(H)]^+$ catalysts (this work) containing nitrogen-based ligands, L.

Despite the fact that ZnO has long since been proposed as the catalyst for formic acid decomposition,[14] zinc-based catalysts are not yet commonly employed. Thus, we were intrigued by recent reports of zinc-based catalysts by Parkin and co-workers. For example, the zinc hydride complex [Tptm]ZnH (where Tptm = tris(2-pyridylthio)methyl anion) reacts with formic

acid to produce molecular hydrogen and [Tptm]Zn(O_2CH).[15] [Tptm]Zn(H) also readily reacts with CO_2 to form the formate complex [Tptm]Zn(O_2CH), [16] which is the reverse reaction of step **II** in Scheme 1A and represents a key step in catalytic cycles for the production of formic acid via hydrogenation of CO_2. Here we use gas-phase studies to evaluate the efficiency of a series of zinc-based $[(L)Zn(H)]^+$ catalysts with various N-based ligands L (Scheme 1F) in decomposing gaseous formic into molecular hydrogen and carbon dioxide as well as in the reverse CO_2 reaction with hydrides $[(L)Zn(H)]^+$. In order to study the role of denticity, we compare the reactivity of the complexes with the tridentate ligand, 2,2';6',2''- terpyridine (tpy, **a**) to those with the bidentate ligands 2,2'-bipyridyl (bpy, **b**) and 1,10-phenanthroline (phen, **c**).

Experimental

Materials

Zinc acetate, 2,2';6',2''- terpyridine (tpy), 2,2'-bipyridyl (bpy), 1,10-phenanthroline (phen), formic acid were all purchased from Sigma-Aldrich (St. Louis, MO, USA) and used as received. Samples were prepared by mixing equal volumes of zinc acetate (5 mM in methanol) and stock solutions of the auxiliary ligands (1 mg/mL in methanol). A volume of formic acid equal to 10% of the zinc/ligand solution volume was then added to the mixture. The sample was allowed to react for 10 min to allow the formation of the formate complex and then diluted to a final complex concentration of 0.5 mM with methanol. Solutions prepared by this method were directly injected into the mass spectrometer through an electrospray ion source.

Methods

Mass spectrometry

Gas-phase experiments involving formic acid were carried out on a Bruker Esquire 3000 quadrupole ion trap mass spectrometer (Bruker Daltonics, Bremen, Germany) custom modified to perform ion molecule reactions (IMR); the modification is thoroughly described elsewhere.[17] The samples were introduced via electrospray ionization (ESI) to the mass spectrometer at a flow rate of 3.0 μL/min. Source parameters were set to 12 PSI for the nebulizer gas and 4.0 kV for the needle voltage. The source temperature was maintained at 250 ^{o}C. The formate precursor ions, $[(L)Zn(O_2CH)]^+$, were isolated using a window of about 1 m/z and subjected to collision-induced dissociation (CID) using fragmentation amplitudes that ranged from 0.2 to 0.5 V. Fragmentation was optimized in each case to maximize the product ion signal of the hydride complex, $[(L)Zn(H)]^+$, while ensuring that about 10% of the precursor ion remained intact. Energy-resolved CID experiments were carried out for the decarboxylation of the $[(L)Zn(O_2CH)]^+$ complexes **2a**, **2b** and **2c** by varying the CID fragmentation amplitudes using a activation time of 30 ms. The applied CID voltage required to dissociate 50% of the precursor ion (in this case $[(L)Zn(O_2CH)]^+$) was designated as $E_{1/2}$.

The neutral vapours of formic acid were introduced through a leak valve. The reaction time was varied by changing the scan delay in the range of 30-1500 ms. Pressure of the formic acid was calculated through calibration based on a known rate of reaction of $[(dppm)Ag_2(H)]^+$.[13a]

Ion-molecule reactions with CO_2 were carried out on a Thermo Finnigan (San Jose, CA) linear ion trap (LTQ) mass spectrometer. Neutral 1% CO_2 in helium (Air Gas, Radnor, PA) was delivered to the ion trap via a bypass on the instrument helium line.[18] The decarboxylation and formation of the zinc hydride complex was done through CID using a normalized collision energy of 10% with an activation time of 30 ms. CID isolation width was set at 2 m/z. Pressure of CO_2 was taken as 1% of the normal ion trap operating He pressure (1.75×10^{-3} Torr as provided by the manufacturer). In order to compare the ion structures of the product of reaction of $[(L)Zn(H)]^+$ with CO_2 to the authentic formate structure, $[(L)Zn(O_2CH)]^+$, energy-resolved CID experiments were carried out to compare the profiles and $E_{1/2}$.

Computational methods

All calculations were performed using Gaussian 09.[19] Initial optimizations of the geometries and energies of reagents and products were done on samples of $[(L)Zn(O_2CH)]^+$, and $[(L)Zn(H)]^+$ with L= **a**, **b**, **c**. In order to evaluate the consistency and reliability of different computational methods to this particular problem, seven combinations of HF/DFT models and basis sets (HF/6-31+G(d,p), M06L/6-311+G(d,p), M11L/6-311+G(d,p), M06L/6-311+G(2df,p) (Zn) + 6-311+G(d,p) (other atoms), M11L/6-311+G(2df,p) (Zn) + 6-311+G(d,p) (other atoms), M06L/cc-pVTZ-pp (Zn) + cc-pVTZ (other atoms), M11L/cc-pVTZ-pp (Zn) + cc-pVTZ (other atoms)) were used to model structures and energetics of reactants and products. As a perturbation theory check on the DFT results, MP2/6-311+G(d,p)//M06L/6-311+G(d,p) single point energies were determined for reactants, products, and key transition states. Energetic data for all model chemistries appear in Supporting Information Table S1. We observed that energy differences along the potential energy surface changed little for DFT model chemistries higher than M06L/6-311+G(d,p). The MP2 energies tended to be more exothermic for IMR processes and the associated barriers, and more endothermic for CID processes and their associated barriers. However, they were not sufficiently different from the DFT results to suggest systemic problems with the latter, so structural data and energies from the M06L/6-311+G(d,p) model chemistry are discussed below. Vibrational frequencies at this level were computed for each of the structures to ensure that the structure was either a minimum (no imaginary frequencies) or a transition state (one imaginary frequency), and to provide thermodynamic corrections to the raw energies. Test counterpoise calculations on formate complexes indicated that the magnitude of the basis set superposition error (BSSE, M06L/6-311+G(d,p) level) was small (~ 3-4 kJ/mol). Consequently

the data were not corrected for BSSE. The M11L/cc-pVTZ-pp + cc-pVTZ wavefunctions were used with Natural Bond Orbital (NBO) and Quantum Theory of Atoms In Molecules (QTAIM) analyses to obtain atomic charges.

Results and discussion

Electrospray ionization (ESI) MS of solutions containing zinc acetate, one of the N-based ligands shown in Scheme 1F and formic acid resulted in the desired zinc formate complexes, **2**, which undergo decarboxylation to form the desired zinc hydride complexes, **1**. In the next sections we describe the results of gas-phase experiments and DFT calculations that probe the following three reactions: (1) **step I** of the catalytic cycle (Scheme 1A) in which the zinc hydride complexes, **1** react with formic acid to liberate hydrogen and generate the carboxylate complexes, **2** (Eq. 4); (2) **step II** of the catalytic cycle in which the zinc hydride complexes, **1** are regenerated via CID on the carboxylate complexes, **2** (Eq. 5); (3) the carboxylation of $[(L)Zn(H)]^+$ via IMR with CO_2 (Eq. 6), which represents the reverse of the decarboxylation reaction (Eq. 5).

$$[(L)Zn(H)]^+ + HCO_2H \rightarrow [(L)Zn(O_2CH)]^+ + H_2 \quad \text{(Eq. 4)}$$

$$[(L)Zn(O_2CH)]^+ \rightarrow [(L)Zn(H)]^+ + CO_2 \quad \text{(Eq. 5)}$$

$$[(L)Zn(H)]^+ + CO_2 \rightarrow [(L)Zn(O_2CH)]^+ \quad \text{(Eq. 6)}$$

(1) Reaction of the zinc hydride complexes $[(L)Zn(H)]^+$, 1, with formic acid.

In all cases, the mass-selected complexes $[(L)Zn(H)]^+$ reacted selectively with formic acid to form the formate complexes $[(L)Zn(O_2CH)]^+$ with concomitant liberation of hydrogen (Eq. 4) as shown in Figure 1, which compares the extent of the reaction for complexes **1a** – **1c** with formic acid at a reaction time of 1000 ms. Conversion of $[(tpy)Zn(O_2CH)]^+$, **1a** , to the formate complex is the most advanced, higher than 60%. In contrast, for the same reaction time, less than 20% of conversion to the formate complexes occurs for $[(bpy)Zn(O_2CH)]^+$, **1b** and $[(phen)Zn(O_2CH)]^+$, **1c**. Full kinetic data, i.e., bimolecular rate constants for the reaction of $[(L)Zn(H)]^+$ with formic and reaction efficiencies (ratio of the experimental rate constant to the collision rate constant) are given in Table 1 and Figure S4 and establish a quantitative reactivity order of: **1a** (φ = 100%) >> **1c** (φ = 8.5%) ≈ **1b** (φ = 4.9%), where **1c** and **1b** are statistically indistinguishable given the experimental uncertainty (30%) in the pressure.

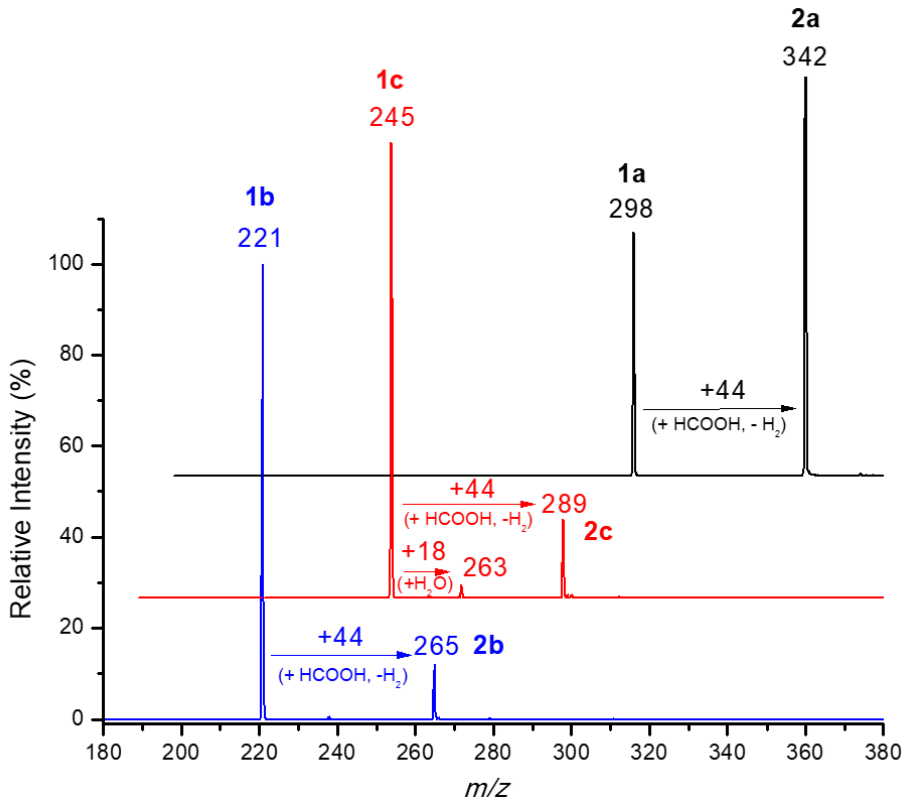

Fig. 1. Spectra of the ion molecule reactions of **1a, 1b** and **1c** ($[(L)Zn(H)]^+$) with neutral formic acid (P= 4.6 *10^{-8} Torr) taken after 1000 ms of reaction time.

The ion-molecule reactions of formic acid with $[(L)Zn(H)]^+$ to produce $[(L)Zn(O_2CH)]^+$ and H_2 (Eq. 4) must be exothermic processes with activation energies that lie below the separated reactants[20] in order for them to occur under the near thermal conditions of the ion trap.[21] Indeed, DFT calculations reveal this to be the case, with the reaction proceeding via a classic Brauman double well potential [22] (Figure 2 for $[(tpy)Zn(H)]^+$, **1a**, and Supporting Information Figures S5 and S7 for **1b** and **1c**, respectively). An initial encounter complex, **3a**, is formed which then proceeds over a single transition state **TS(3a-4a)** to yield the product ion-molecule complex **4a**, which then loses H_2 to form the formate complex **2a**. Formation of **2a** is predicted to be exothermic in all cases. The activation barriers associated with **TS(3L-4L)** (i.e. **3** → **TS**) vary somewhat with L, with tpy (19 kJ/mol) < phen ≈ bpy (40, 41 kJ/mol) (Table 1). This matches the experimental reactivity rate of the zinc complexes.

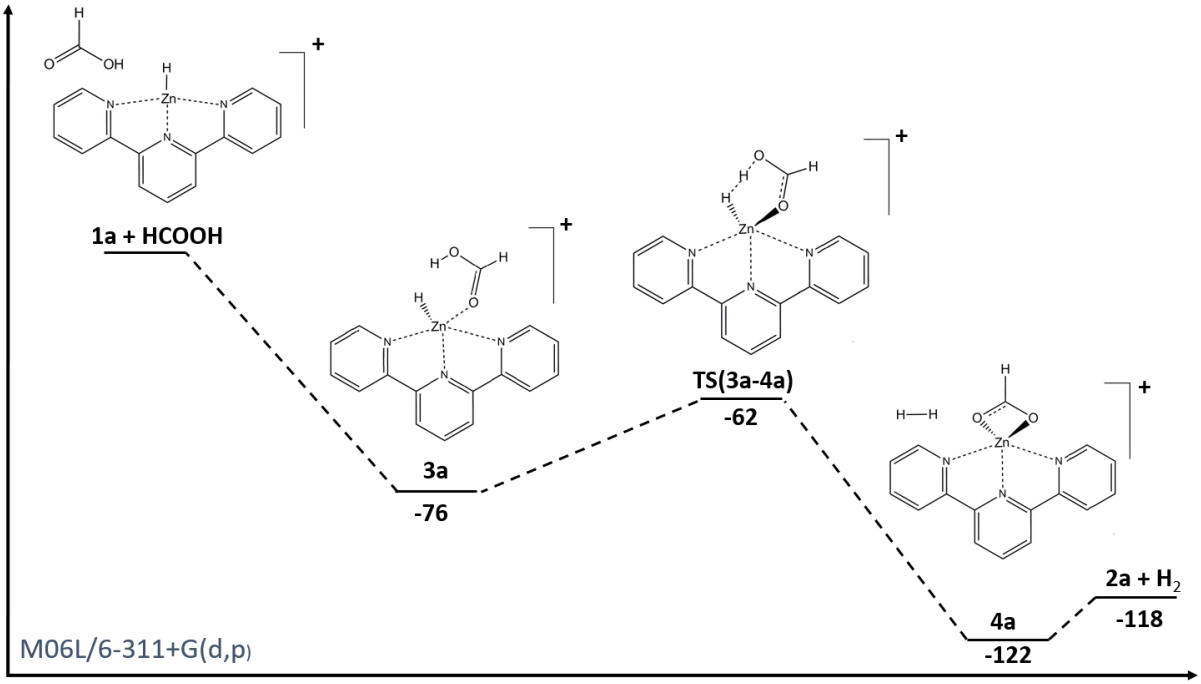

Fig. 2. Calculated (M06L/6-311+G(d,p)) reaction mechanism for the dehydrogenation of **1a** (Eq.4). Energies are reported in kJ/mol and include ZPE.

Table 1. (**A**) Experimental bimolecular rate constants (k_2)[a] and relative collision reaction efficiencies (φ)[b] for the dehydrogenation reaction of ions **1a**, **1b**, and **1c** (Eq. 4); **(B)** Thermochemical values (ΔH^o_{298} and ΔG^o_{298}, and ΔE) associated with formic acid dehydrogenation (Eq.4) as L varies; **(C)** Energies relative to the separate reactants of each of the reaction geometries found for the reaction mechanism pathways (Eq. 4 and Fig. 2). All energies are calculated at the M06L/6-311+G(d,p) level of theory and are reported in kJ/mol inclusive of the ZPE.

	(A)		**(B)**			**(C)**				
Ligand (L)	k_2 [(a)]	φ [(b)]	ΔH^o_{298}	ΔG^o_{298}	ΔE(TS(3L-4L) -3L)	1L+ HCO_2H	ΔE (3L)[c]	ΔE (TS(3L-4L))[c]	ΔE(4L)[c]	ΔE(2L+H_2)[c]
a	1.3*10^{-9}	100	-112	-99	14	0	-76	-62	-122	-118
b	6.5*10^{-11}	4.9	-79	-69	41	0	-75	-34	-88	-85
c	1.1*10^{-10}	8.5	-80	-68	40	0	-75	-35	-89	-86

[a] The rate constants represent the average of three independent measurements and errors are conservatively estimated as ±30%, in units of: cm^3 molecules^{-1} s^{-1}.

[b] Reaction efficiency (φ) = k_2/k_{Cap} × 100%. The collision rate k_{Cap} was calculated using the theory of Su and Chesnavich.[23]

[c] Energies are in kJ/mol and are relative to the separated reactants.

Examination of the geometries of the intermediate **3a** and **TS(3a-4a)** reveals key parameters associated with the reaction coordinate. In **3a** the carbonyl oxygen of the formic acid coordinates to the Zn thereby bringing the acidic hydrogen on the formic acid toward the hydridic Zn-H. The distortion of the H-Zn-O (104.9°) and the Zn-O-C (120.9°) angles and the elongation of the Zn-H bond from 160 to 170 pm due to the non-covalent interactions between the opposite partial charges on the two H atoms which face each other at a distance of 180 pm

allows the system to move toward **TS(3a-4a)**, see Fig. 2. Here the once hydroxylic hydrogen oscillates along the O-H-H bond axis around its equilibrium distances of 140 pm from the oxygen and 90 pm from the hydridic hydrogen. As the distance decreases, the strength of the interaction of the two hydrogen atoms increases and ultimately the system relaxes by expelling molecular hydrogen and yielding $[(L)Zn(O_2CH)]^+$ **(2a)**. The respective geometries for the complexes with ligands **b** and **c** are given in Figs. S5 and S7.

Population and charge analyses were performed using NBO and QTAIM methods (Table 2). Charge values on the hydrogen atom of the hydride (-0.38 for **1a** and -0.31 for **1b** and **1c,** QTAIM calculated charges) reveal a direct correlation between the negative charge on the hydrogen and the observed experimental reactivity in that **1a** with a more negative charge results in faster reaction (**1a**). Overall, this information suggests that the ligand-induced negative charge on the hydrogen is crucial in tuning the reactivity of the ligated zinc hydride ion. The stronger electron-donating ability of the tridentate tpy ligand **a** enhances the hydridic nature of the hydrogen and reduces the barrier to the deprotonation of formic acid.

Table 2. Metal – hydrogen bond distance and trends of partial charges distribution on the hydridic hydrogen calculated with four methods at M11L/cc-pVTZ-pp + cc-pVTZ level of theory add Zn-H distance

		Zn-H	H charge (e^-)	
		(pm)	NBO	QTAIM
1a	$[(tpy)Zn(H)]^+$	155	-0.37	-0.38
1b	$[(phen)Zn(H)]^+$	152	-0.33	-0.31
1c	$[(bpyn)Zn(H)]^+$	152	-0.33	-0.31

(2) Decarboxylation reactions of the zinc formate complexes $[(L)Zn(O_2CH)]^+$, 2.

The mechanism of collision-induced decarboxylation of ions $[(L)M_n(O_2CH)]^+$ has been well defined in the literature for bimetallic complexes.[13a] Figure 3 shows the calculated potential energy surface for a plausible mechanism for the collision-induced decarboxylation (Eq. 5) of **2a**.

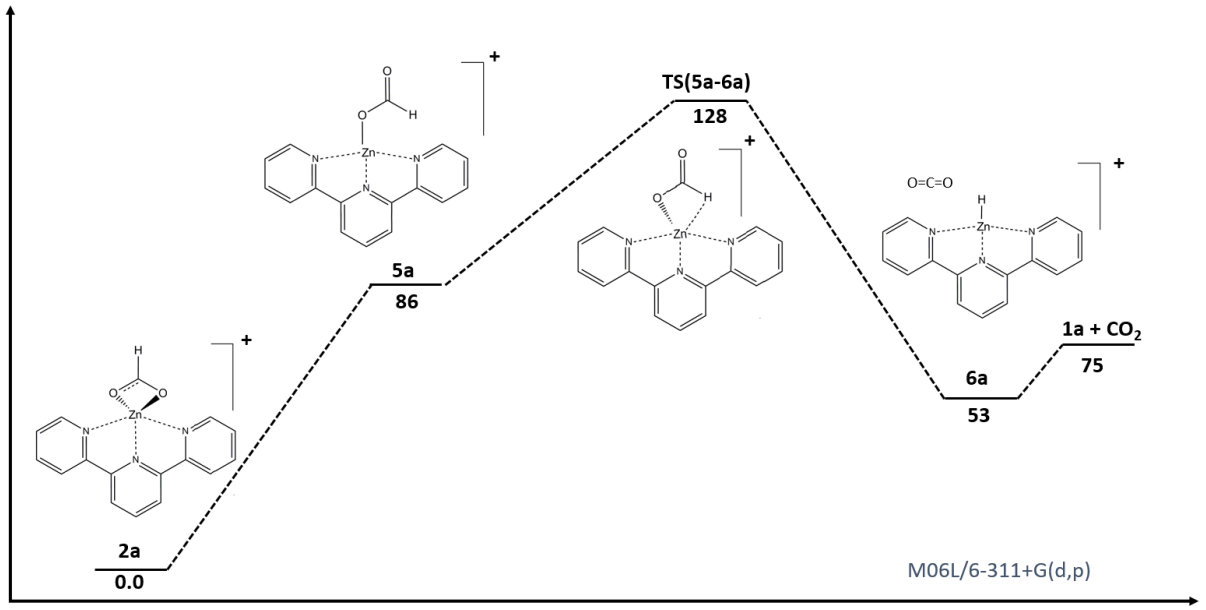

Fig. 3. Calculated (M06L/6-311+G(d,p)) reaction mechanism for the decarboxylation of **2a** (Eq.5). Energies are reported in kJ/mol and include ZPE.

In the case of $[(tpy)Zn(O_2CH)]^+$ the model shows that the pentacoordinated complex (**2a**) undergoes rotation of the formate moiety along one of the C-O bond. Consequently, one of the Zn-O bond breaks, and the species **5a** (formate bound to Zn as a monodentate ligand) is formed. We were not able to locate a transition state for this step.

The reaction then progresses to the critical transition state, **TS(5a-6a)**, which sees the hydrogen oriented perpendicularly to the molecular plane beginning its interaction with the metal centre. As the bond between the hydrogen and the zinc becomes stronger, both Zn-O and C-H stretch until the ejection of neutral CO_2 restores $[(L)Zn(H)]^+$ (**1a**). This step goes via the formation of the ion-molecule complex between **3a** and CO_2 (**6a**) before yielding the separated products. Similar reaction profiles were calculated for the decarboxylation of **2b** and **2c**. They

are shown in Supplemental Information (Figures S6 and S8, respectively). The M06L/6-311+G(d,p) calculated activation energies for the decarboxylation reaction of ions **2a**, **2b**, and **2c** are very similar (~130 kJ/mol, Table 3).

We also performed RRKM calculations[24] to compare the unimolecular rates for the decarboxylation of ions **2a**, **2b**, and **2c** as a function of ion energy. The predicted rates (Figure S9) follow the order **2c** ≈ **2b** > **2a**. This is consistent with the similar activation barriers calculated for these reactions, as ion **2a** has significantly more vibrational degrees of freedom due to the bigger ligand size. Experimentally, $E_{1/2}$ values for ions **2a**, **2b**, and **2c** obtained via energy-resolved CID experiments, are consistent with the RRKM data: Ion **2a** had $E_{1/2}$ value of 0.58V, compared to 0.49 and 0.52V for ions **2b** and **2c,** respectively, indicating that **2a** requires more energy to achieve the same level of decarboxylation.

Table 3. **(A)** Calculated thermochemical values (ΔH^{o}_{298} and ΔG^{o}_{298}, and E_a) associated with the decarboxylation reaction (Eq.5); **(B)** Calculated energies relative to the reactant (**2L**) for each of the reaction species and intermediates (Eq. 5; Fig. 3). All computational values are calculated at the M06L/6-311+G(d,p) level of theory and are reported in kJ/mol and include ZPE.

		(A)			**(B)**			
Ligand (L)		**ΔH^0_{298}**	**ΔG^0_{298}**	**E_a**	**ΔE(2L)**	**ΔE(5L)**	**ΔE(TS(5L-6L))**	**ΔE(6L)**
a		76	33	128	0	86	128	53
b		42	4	130	0	93	130	17
c		43	2	131	0	94	131	18

The decarboxylation reaction (Eq. 5) is expected to be endothermic, and the calculations performed at the M06L 6-311+G(d,p) level of theory (Table 3) found that the reaction endothermicity $\Delta H°_{298}$ = 74 kJ/mol is higher for **2a** than those for **2b** or **2c,** (42 and 41 kJ/mol,

respectively). Complete calculated energetics for all intermediate species for each of the three ligands are given in Table 3.

(3) Reaction of the zinc hydride complexes $[(L)Zn(H)]^+$, 1, with formic acid.

The decarboxylation reaction (Eq. 5) of the formate complex was found to be reversible in the gas phase. When allowed to react with CO_2 gas, the hydride complex **1a** (*m/z* 298) underwent addition of 44 Da via ion-molecule reaction to form a *m/z* 342 product, which either corresponds to the ion-molecule complex, $[(tpy)Zn(H)(CO)_2]^+$, or the formate complex, $[(L)Zn(O_2CH)]^+$ (Fig. S1). To establish that the reaction product was in fact the formate complex produced via insertion of carbon dioxide into Zn-H bond (as shown in Eq. 6), energy-resolved CID experiments were performed. We compared CID decarboxylation of two *m/z* 342 ions: **2a** formed by ESI from solution and the species observed after IMR of **1a** with CO_2. Figure S2 shows the energy-resolved CID profiles for these two ions. The similarities of the profiles as well as the $E_{1/2}$ values, which are within 0.5% of normalized collision energy, strongly suggest that they belong to the same chemical species. Similar results were obtained for the ions **2b** and **2c** compared to the products of the carboxylation reactions of **1b** and **1c**. Additional experiments were done to rule out simple ion-molecular complex formation. For example, complexes $[(L)Zn]^{2+}$ did not form an adduct with CO_2 under our experimental conditions (data not shown). Thus, we conclude that the product of Eq. 6 is indeed the formate complex $[(L)Zn(O_2CH)]^+$.

This allows us to apply the principle of microscopic reversibility to the mechanism found for Eq. 5 (Figure 3) to the $[(L)Zn(H)]^+$ carboxylation reaction and thereby use the DFT calculated energetics (Figures 3, S6 and S8) previously discussed for the decarboxylation reactions. The CO_2 insertion reaction (Eq. 6) is exothermic and the barrier in the case of L= **a** is 52 kJ/mol compared to the separated reactants. This is a significant barrier and causes the reaction to be very slow. The experimental rate constant of reaction of **1a** with CO_2 was estimated (Fig. S3) and its efficiency is quite low, 4×10^{-4} %, as reported in Table 4. Reactions of **1b** and **1c** were estimated to be 13 and 3 times slower, respectively. This is in agreement with the barriers for L = **b** and **c** being substantially higher (88 kJ/mol, Table 4). These reaction rates are very slow and are normally outside the range of what can generally be measured in ion trap mass spectrometers. We are aided by a couple of factors – the pressure of CO_2 is very high ($\sim 10^{-5}$ Torr), and the $[(L)Zn(H)]^+$ complexes do not seem to react with background gases (typically H_2O, N_2 and O_2) fast enough to compete with the carboxylation reaction. Even under these

conditions we are only sampling the initial kinetics and unable to collect data across a single half-life of the reaction.

Table 4. (A) Experimental bimolecular rate constants (k_2") and reaction efficiencies for the carboxylation reaction (Eq. 6) of ions **1a**, **1b**, and **1c**. **(B)** Energies (relative to the separate reactants, **1** and CO_2) of each of the reaction species and intermediates (Eq. 6 and the mechanism reverse of one shown in Fig. 3). All energies are calculated at the M06L/6-311+G(d,p) level of theory and are reported in kJ/mol inclusive of the ZPE.

	(A)		**(B)**		
Ligand (L)	k_2" [a]	φ [b]	ΔH^0_{298}	ΔG^0_{298}	E_a
a	$3.0*10^{-15}$	$4*10^{-4}$	-76	-33	52
b	$2.0*10^{-16}$	$3*10^{-5}$	-42	-4	88
c	$1.0*10^{-15}$	$1*10^{-4}$	-43	-2	88

[a] The rate constants represent the average of three independent measurements and errors are conservatively estimated as ±30%,in units of: cm^3 $molecules^{-1}$ s^{-1}.

[b] Reaction efficiency (φ) = k_2/k_{Cap} × 100%. The collision rate k_{Cap} was calculated using the theory of Su and Chesnavich.[23]

A correlation between Zn-H bond length and the reactivity of neutral Zn complexes in carboxylation reactions has been reported in the literature.[41] [Tm^{But}]Zn(H), for example is known to react easily with CO_2 and its Zn-H bond length is 147 pm. Longer bond distances (within the common range of 144-177 pm), have been shown to result in lower reactivity requiring higher temperatures.[25]

In our case (charged, gas-phase) with all three ligands the calculated Zn-H distances are similar (152- 155 pm, Table 4). The ionic nature of the systems allows for a more pronounced localization of the negative charge onto the hydrogen and the magnitude of this negative charge seems to have a more pronounced effect on reactivity than the Zn-H distance.

In solution, the ability of a species to participate in hydride donation to CO_2 can be evaluated by measuring the $\Delta G°_{H-}$, or hydricity. If this value is lower than the $\Delta G°_{H-}$ of the

accepting species, in this case formate (184 kJ/mol in acetonitrile) the carboxylation reaction (Eq. 3) will occur.[26] Most of the species with hydricity values favourable to donate hydride to CO_2 are complexes derived from the metals Ir, Ru, Rh, and Pt.[26]

This type of hydricity consideration is valid for reactions resulting in separated products, i.e., reaction in Eq. 7:

$$[(L)M(H)]^{n+} + CO_2 \rightarrow [(L)M]^{(n+1)+} + HCO_2^- \quad \text{(Eq. 7)}$$

If the formate anion stays coordinated to the metal centre (thus forming $[(L)M(O_2CH)]^{n+}$, Eq. 6 as example), it results in additional stabilization. This allows species with lower hydricity values to hydrogenate CO_2. Fong and Peters[27] showed that several iron hydride complexes with hydricity values around 230 kJ/mol did react with CO_2 in solution under mild conditions. Our gas-phase study produces the same type of formate complex, ion **2**, formation of which is in part responsible for driving the insertion of CO_2 (Eq. 6).

Conclusions

Zn complexes, in the form of $[(L)Zn(H)]^+$, where L is a nitrogen-containing ligand, were found to be effective catalysts for the selective decomposition of formic acid in the gas phase. As the ligand L was varied, a range of reactivities was observed. The tridentate aromatic nitrogen-containing ligand terpyridine (**a**) yielded the fastest reaction rates among the ligands tested in this work. $[(tpy)Zn(H)]^+$ displayed nearly collision reaction efficiency for the dehydrogenation of formic acid, which compares favourably with other gas-phase systems previously described. [13a]

Computational evaluations of reaction energetics and transition states agreed with the experimental reaction efficiencies. Thus, the DFT-calculated barriers highlighted the same ligand-reactivity relationships as the experimentally observed ones. Even though the mechanisms were shown to be very similar for all three ligands studied, the difference in reactivities can be attributed to a ligand-dependent magnitude of the activation barriers. Furthermore, experimental reaction rates and partial charge distribution values were found to correlate; the stronger electron-donating ability of the tridentate ligand tpy (**a**) enhances the hydridic nature of the hydrogen and reduces the barrier to the deprotonation of the formic acid.

The catalyst ions **1**, $[(L)Zn(H)]^+$, can be easily reformed by decarboxylation of the formate complex **2**, $[(L)Zn(OOCH)]^+$. It is important to note that in the case of these zinc-based catalysts, decarboxylation (Eq. 5) is reversible. The zinc systems reported in this work contrast with known coinage metal catalysts for the application on formic acid decomposition in the gas phase,[13a,c] showing that combining abundant metals and simple ligands can create more efficient and affordable catalysts.

ACKNOWLEDGEMENTS

This work was supported by the Department of Chemistry and Biochemistry, Northern Illinois University. RAJO thanks the Australian Research Council for financial support (DP180101187). We thank Ms. Shanshan Guan for help with the RRKM calculations.

References

(1) a) P. Sabatier, A. Mailhe, *Compt. Rend.* **1912,** 152, 1212–1215.; b) P. Sabatier, Catalysis in organic chemistry. Translated by Reid, E. E., Library Press, London **1923**.; c) P. Mars, J. J. F. Scholten, P. Zwietering, *Adv. Catalysis* **1963,** 14, 35–113 d) J. M. Trillo, G. Munuera, J. M. Criado, *Cat. Rev.* **1972**, 7, 51.

(2) a) W.A. Herrmann, M. Muehlhofer, Applied Homogeneous Catalysis with Organometallic Compounds, B. Cornils and W.A. Herrmann (Eds), Wiley-VCH, Weinheim, 2nd Edition, **2002**, Volume 3, 1086. b) C. Odabasi, M. E. Gunay, R. Yildirim, *Int. J. Hydrogen Energy* **2014,** 39, 5733– 5746.

(3) K. Saito, T. Shiose, O. Takahashi, Y. Hidaka, F. Aiba, K. Tabayashi, *J. Phys. Chem. A* **2005,** 109, 5352–5357.

(4) a) B. Wang, H. Hou, Y. Gu, *J. Phys. Chem. A* **2000,** 104, 10526–10528. b) J.-G. Chang, H.-T. Chen, S. Xu, M. C. Lin, *J. Phys. Chem. A* **2007,** 111, 6789–6797.

(5) a) M. Grasemann, G. Laurenczy, *Energy Environ. Sci.* **2012**, 5, 8171–8181. b) A. Boddien, F. Gärtner, C. Federsel, P. Sponholz, D. Mellmann, R. Jackstell, H. Junge, M. Beller, *Angew. Chem., Int. Ed.* **2011,** 50**,** 6411–6414. c) S. Enthaler, J. von Langermann, T. *Energy Environ. Sci.* **2010**, 3, 1207–1217.

(6) B. Loges, A. Boddien, F. Gärtner, H. Junge, M. Beller, *Top. in Cat.* **2010**, 53, 902–914.

(7) D. J. Braden, C. A. Henao, J. Heltzel, C. T. Maravelias, J. A. Dumesic, *Green Chem.* **2011**, 13, 1755–1765.

(8) Q.-Y. Bi, X.-L. Du, Y.-M. Liu, Y. Cao, H.-Y. He, K.N. Fan, *J. Am. Chem. Soc.* **2012**, 134, 8926–8933.

(9) a) J. Boddien, *Nature Nanotech.* **2011**, 6, 265–266. b) K. Tedsree, L. Tong, S. Jones, C. A. Wong, K.M.K. Yu, P. A. J. Bagot, E.A. Marquis, G. D. W. Smith, S. C. E. Tsang, *Nature Nanotech.* **2011**, 6, 302–307.

(10) a) R. A. J. O'Hair, *Chem. Comm.*, **2006**, 1469 – 1481; b) R. A. J. O'Hair, N. J. Rijs, *Acc. Chem. Res.*, **2015**, *48*, 329–340; c) R. A. J. O'Hair, *Int. J. Mass Spectrom.*, **2015**, *377*, 121–129.

(11) a) K. L. Vikse, J. S. McIndoe, *Pure Appl. Chem*. **2015**, 87, 361. b) K. L. Vikse, Z. Ahmadi, J. S. McIndoe, *Coord. Chem. Rev.* **2014**, 279, 96.

(12) G. N. Khairallah, R. A. J. O'Hair, *Int. J. Mass Spectrom.* **2006**, 254 (3), 145–151.

(13) a) A. Zavras, G. N. Khairallah, M. Krstić, M. Girod, S. Daly, R. Antoine, P. Maitre, R. J. Mulder, S.-A. Alexander, V. Bonačić-Koutecký, *Nat. Commun.* **2016**, *7*, 11746. b) A. Zavras, J. M. White, R. A. J. O'Hair, *Dalt. Trans.* **2016**, *45* (48), 19408–19415. c) A. Zavras, M. Krstić, P. Dugourd, V. Bonačić-Koutecký, R. A. J. O'Hair, *ChemCatChem* **2017**, *9* (7), 1298–1302. d) M. Krstić, Q. Jin, G. N. Khairallah, R. A. J. O'Hair, V. Bonačić-Koutecký, *ChemCatChem* **2018**, *10* (5), 1173–1177.

(14) a) J. M. Vohs, M. A. Barteau, *Surf. Sci.* **1986**, *176* (1–2), 91–114. b) Y. Noto, K. Fukuda, T. Onishi, K. Tamaru, *Trans. Faraday Soc.* **1967**, *63* (0), 3081.

(15) M. Rauch, Y. Rong, W. Sattler, G. Parkin, *Polyhedron* **2016**, *103*, 135–140.

(16) M. Rombach, H. Brombacher, H. Vahrenkamp, *Eur. J. Inorg. Chem.* **2002**, (1), 153–159.

(17) Y. Pyatkivskyy, V. Ryzhov, *Rapid Commun. Mass Spectrom.* **2008**, *22* (8), 1288–1294.

(18) M. L. Parker, S. Gronert, *Int. J. Mass Spectrom.* **2017**, *418*, 73–78.

(19) V. Barone, C. Latouche, D. Skouteris, F. Vazart, N. Balucani, C. Ceccarelli, B. Lefloch, *Mon. Not. R. Astron. Soc. Lett.* **2015**, *453* (1), L31–L35.

(20) P. D. Dau, P. B. Armentrout, M. C. Michelini, J. K. Gibson *Phys. Chem. Chem. Phys*. **2016**, 18,7334.

(21) a) S. Gronert, *J. Am. Soc. Mass Spectrom.*, **1998**, *9*, 845-848; b) W. A. Donald, G. N. Khairallah, R. A. J. O'Hair, *J. Am. Soc. Mass Spectrom.*, **2013**, *24*, 811-815

(22) J. I. Brauman, *J. Mass Spectrom.*, **1995**, 30, 1649–1651.

(23) T. Su, W. J. Chesnavich, *J. Chem. Phys*., **1982**, 76, 5183

(24) a) C. Lifshitz, Chem. Soc. Rev., 2001, 30, 186–192. b) 80 R. G. Gilbert and S. C. Smith, Theory of Unimolecular and Recombination Reactions, Blackwell Scientific Publications,1990. c) T. Beyer and D. R. Swinehart, ACM Commun., 1973, 16, 379.

(25) A. Kreider-Mueller, P. J. Quinlivan, M. Rauch, J. S. Owen, G. Parkin, *Chem. Comm.* **2016**, *52*(11), 2358–2361.

(26) K. M. Waldie, A. L. Ostericher, M. H Reineke, A. F. Sasayama, C. P. Kubiak, *ACS Cat.* **2018**, *8*(2), 1313–1324.

(27) H. Fong, J. C. Peters, *Inorg. Chem.* **2014**, *54*(11), 5124–5135.

TOC graphic.